




Kaposi's Sarcoma-Associated Herpesvirus Latency Locus Renders B Cells Hyperresponsive to Secondary Infections

Sang-Hoon Sin,^a Anthony B. Eason,^a Rachele Bigi,^a Yongbaek Kim,^b SunAh Kang,^a Kelly Tan,^a Tischen A. Seltzer,^a Raman Venkataramanan,^c Hyowon An,^d  Dirk P. Dittmer^a

^aDepartment of Microbiology and Immunology, Programs in Global Oncology and Virology, Lineberger Comprehensive Cancer Center and Center for AIDS Research, The University of North Carolina at Chapel Hill, Chapel Hill, North Carolina, USA

^bLaboratory of Veterinary Clinical Pathology, College of Veterinary Medicine, Seoul National University, Seoul, South Korea

^cDepartment of Pharmaceutical Sciences, University of Pittsburgh, Pittsburgh, Pennsylvania

^dDepartment of Statistics & Operations Research, The University of North Carolina at Chapel Hill, Chapel Hill, North Carolina, USA

ABSTRACT Kaposi's sarcoma-associated herpesvirus (KSHV) induces B cell hyperplasia and neoplasia, such as multicentric Castleman's disease (MCD) and primary effusion lymphoma (PEL). To explore KSHV-induced B cell reprogramming *in vivo*, we expressed the KSHV latency locus, inclusive of all viral microRNAs (miRNAs), in B cells of transgenic mice in the absence of the inhibitory FcγRIIB receptor. The BALB/c strain was chosen as this is the preferred model to study B cell differentiation. The mice developed hyperglobulinemia, plasmacytosis, and B lymphoid hyperplasia. This phenotype was ameliorated by everolimus, which is a rapamycin derivative used for the treatment of mantle cell lymphoma. KSHV latency mice exhibited hyperresponsiveness to the T-dependent (TD) antigen mimic anti-CD40 and increased incidence of pristane-induced inflammation. Lastly, the adaptive immunity against a secondary infection with Zika virus (ZIKV) was markedly enhanced. These phenotypes are consistent with KSHV lowering the activation threshold of latently infected B cells, which may be beneficial in areas of endemicity, where KSHV is acquired in childhood and infections are common.

IMPORTANCE Kaposi's sarcoma-associated herpesvirus (KSHV) establishes latency in B cells and is stringently linked to primary effusion lymphoma (PEL) and the premalignant B cell hyperplasia multicentric Castleman's disease (MCD). To investigate potential genetic background effects, we expressed the KSHV miRNAs in BALB/c transgenic mice. BALB/c mice are the preferred strain for B cell hybridoma development because of their propensity to develop predictable B cell responses to antigen. The BALB/c latency mice exhibited a higher incidence of B cell hyperplasia as well as sustained hyperglobulinemia. The development of neutralizing antibodies against ZIKV was augmented in BALB/c latency mice. Hyperglobulinemia was dampened by everolimus, a derivative of rapamycin, suggesting a role for mTOR inhibitors in managing immune activation, which is hallmark of KSHV infection as well as HIV infection.

KEYWORDS KSHV, Kaposi's sarcoma, mouse model, primary effusion lymphoma, rapamycin

Hyperglobulinemia is a clinical sign of nonspecific immune activation. It is defined as an abnormally high concentration of immunoglobulins (Igs) in peripheral blood (1). This is due to polyclonal B cell activation and an increased number of plasma cells. Hyperglobulinemia is a feature of many human lymphoproliferative diseases, including

Received 6 July 2018 Accepted 6 July 2018

Accepted manuscript posted online 18 July 2018

Citation Sin S-H, Eason AB, Bigi R, Kim Y, Kang S, Tan K, Seltzer TA, Venkataramanan R, An H, Dittmer DP. 2018. Kaposi's sarcoma-associated herpesvirus latency locus renders B cells hyperresponsive to secondary infections. *J Virol* 92:e01138-18. <https://doi.org/10.1128/JVI.01138-18>.

Editor Jae U. Jung, University of Southern California

Copyright © 2018 American Society for Microbiology. All Rights Reserved.

Address correspondence to Sang-Hoon Sin, sang-hoon_sin@med.unc.edu.

multicentric Castleman's disease (MCD) and primary effusion lymphoma (PEL) (2, 3). PEL and the plasmablastic variant of MCD are connected with Kaposi's sarcoma-associated herpesvirus (KSHV) (4, 5). Our understanding as to how KSHV affects B cells during premalignant, latent persistence is incomplete due to a lack of animal models. Thus far, three experimental approaches have been explored for *in vivo* studies: (i) studies in nonhuman primates using the rhesus rhadinovirus model of infection (6, 7), (ii) studies in mice using the murine gamma herpesvirus-68 (MHV-68) model of infection (8–13), and (iii) studies using transgenic mice (14–17). The KSHV LANA promoter is able to drive B-cell-specific expression of a reporter gene in transgenic mice (18). We previously used this insight to generate transgenic mice that encompass the KSHV latency locus (referred to henceforth as latency mice) in the C57BL/6J genetic background (19). These mice displayed hyperresponsiveness to LPS, marginal zone (MZ) expansion, and plasmacytosis followed by hyperglobulinemia and lymphoma. To investigate in detail how the latency locus predisposes B cells to hyperresponsiveness and hyperproliferation, the transgene was moved into the BALB/c background, which is the preferred model to study B cell biology, and the response to various antigens, including Zika virus (ZIKV) infection, was explored.

Hyperglobulinemia in KSHV latency mice is a robust phenotype and well maintained under a variety of physiological conditions such as the lack of endogenous microRNA 155 (miRNA-155), lack of endogenous interleukin-6 (IL-6), or forced expression of Myc (20–22). The genetic background of these earlier studies was C57BL/6J, which is widely used in cancer biology and T cell immunology, but less suitable for studies of B cell immunobiology or B cell autoimmune diseases. The importance of genetic background in genetically engineered mouse models (GEMMs) is well documented (reviewed in reference 23). This led us to explore the latency mice in a strain background that is optimal for the study of B cell immunity. BALB/cAnPt mice develop "oil granuloma," an inflammatory condition, and eventually plasmacytoma upon intraperitoneal (i.p.) injection of pristane (24). This phenotype is the foundation of monoclonal antibody (MAb) production. BALB/cAnPt plasmacytomas develop as ascites in the intraperitoneal cavity mimicking human PEL. The phenotype is dependent on the substrain of BALB/c mice. In addition, Myc, p16INK4a, IL-6, and the microbiome in the environment (colony effects) modulate disease severity (25–27).

B cell expansion is initiated by a variety of different stimuli that engage the B cell receptor (BCR) and either CD40 for T-dependent antigen or BCR/Toll-like receptor (TLR) and BCR/CD19/CD21 (complement receptor) for T-independent (TI) antigens. Experimental protocols to explore these signaling pathways have been extensively validated in the BALB/c background and can be used to probe genetic interactions *in vivo*. First, responsiveness to *Escherichia coli* lipopolysaccharide (LPS) was explored. LPS engages TLR4, and TLR4 mutant (TLR4mt) mice are unresponsive to LPS (28–30). CD19⁺ B cells purified from TLR4 mutant mice are likewise unresponsive. Thus, BALB/c-TLR4 mutant mice were used to test the hypothesis that the polyclonal B cell activation phenotype in KSHV latent genes was dependent on TLR4 and to ask whether KSHV latent genes can complement a TLR4 defect. Second, potential Fc γ receptor interactions were explored. Fc γ receptors bind to antigen-antibody complexes and regulate the immune response. There are four classes of Fc γ receptors: Fc γ RI, Fc γ RIIB, Fc γ RIII, and Fc γ RIV (reviewed in reference 31). Fc γ RIIB (CD32B) is a low-affinity Ig- γ receptor expressed on B cells, which inhibits signaling from the BCR (32) and thus limits the IgG response to periods of acute infection. Fc γ RIIB knockout mice (referred to here as FKO mice) respond with augmented antibody production to antigen exposure (33, 34). Hence, FKO mice were chosen to test the hypothesis that Fc γ RIIB was limiting KSHV-induced hyperglobulinemia. Third, B and T cell immune inactivation is critically dependent on mTOR. Rapamycin and its derivatives are used clinically to suppress CD4 T cell proliferation and IL-4 secretion in solid organ transplantation. They have shown efficacy against KS, MCD, and PEL (35–37), as well as mantle cell lymphoma, and long-term, low-dose regimens suppress human autoimmune disorders that result from abnormal polyclonal B and T cell activation (38–40). Everolimus is a derivative of rapamycin

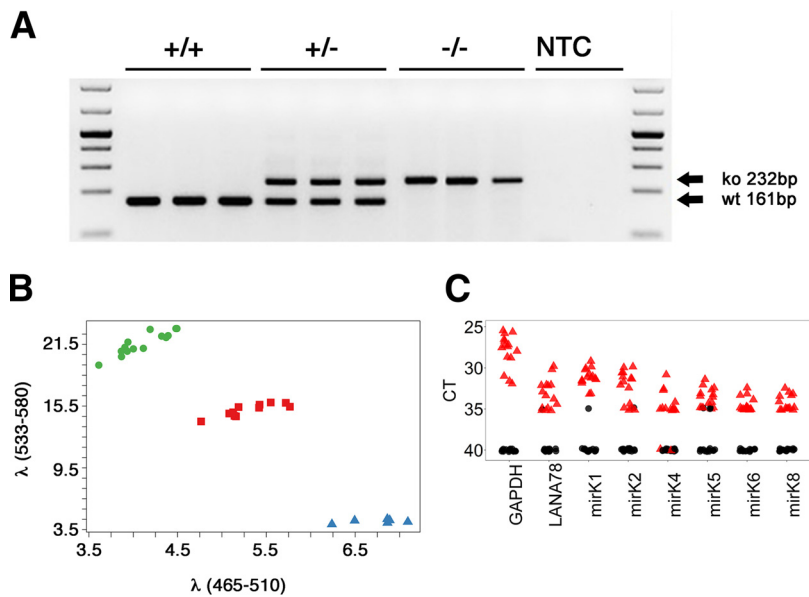


FIG 1 Latency \times FKO and TLR4mt mice. (A) Genotyping of Fc γ RIIB knockout status. +/+, +/-, and -/- represent wild type (WT), hemizygous, and knockout (ko) for the *FCGR2B* gene, respectively. NTC, nontemplate control. (B) Genotyping of a point mutation in TLR4mt mice. The x and y axes indicate fluorescence intensities for the mutant and wild-type *Tlr4* gene, respectively. Clusters of green circles, purple squares, and blue triangles represent the WT, hemizygous, and mutant forms of the *Tlr4* gene, respectively. (C) Transcription of KSHV pre-miRNAs and LANA mRNA in latency \times FKO mice (animals 949, 950, 952, and 956) and a latency \times FKO \times TLR4mt mouse (animal 774). Total RNA from spleen of each mouse was analyzed by RT-qPCR (76). Mouse GAPDH was used as a positive control. The red triangles indicate RT-positive templates and black circles RT-negative templates. The threshold cycle (C_T) number is shown on the vertical axis. Lower C_T values correspond to higher target levels.

(sirolimus) with increased oral bioavailability but exactly the same active core and molecular mechanism. It is rapidly metabolized to rapamycin in blood (41, 42) and was used to test the hypothesis that the long-term administration of low-dose rapamycin can prevent KSHV-induced B cell activation.

Together, the *in vivo* experiments presented here add to our understanding of KSHV-mediated B cell dysregulation during the premalignant (i.e., latent) state. Plasmacytosis and higher incidence of splenic lymphoid hyperplasia (LH) of the C57BL/6J latency mice were augmented in the BALB/c background. Unlike Fc γ RIIB-deleted mice, BALB/c latency mice displayed hyperresponsiveness to anti-CD40 stimulation. The incidence of pristane-induced inflammation was increased in BALB/c latency mice with Fc γ RIIB deleted. The development of neutralizing antibodies against a secondary human pathogen, ZIKV, was augmented in BALB/c latency mice. BALB/c latency mouse hyperglobulinemia was dampened by everolimus, which is an orally available rapamycin analog.

RESULTS

KSHV latency locus induces plasmacytosis and lymphoid hyperplasia. To investigate if the KSHV latency-associated *in vivo* phenotypes were augmented in a more B-cell-active mouse strain, C57BL/6J latency mice were crossed into the BALB/c background for 10 generations. Genotyping was performed as previously described (20). The resultant BALB/c latency mice were then crossed to BALB/c \times FKO mice. Deletion of Fc γ RIIB was assayed by PCR (Fig. 1A). This generated the latency \times FKO line. To assess the effect of the KSHV latency locus in modulating the response to LPS, the *Tlr4*^{Lps-d} allele was introduced into latency \times FKO mice, producing latency \times FKO \times *Tlr4*^{Lps-d} triple mutant mice (referred to here as TLR4mut+). The *Tlr4*^{Lps-d} allele is a point mutant. A C-to-A substitution at position 2342 in the third exon results in a proline-to-histidine change at position 712. Hence, genotyping was performed by allele-specific PCR using probes specific for either the wild-type or mutant allele, each labeled with a

TABLE 1 B cell populations in the BALB/c, BALB/c latency, FKO, latency × FKO, and TLR4mt mice^a

Class ^a	Markers	Frequency of cell population in mouse group													
		BALB/c		BALB/c latency		<i>P</i> vs BALB/c ^b	FKO		Latency × FKO		<i>P</i> vs FKO ^b	Latency × FKO × TLR4mt		<i>P</i> vs latency × FKO ^b	
		%	SD	%	SD		%	SD	%	SD		%	SD		
Mature	CD19 ⁺ IgM ⁺ IgD ⁺	33	3.2	30	4.3	NS	36	2.0	35	4.2	NS	39	3.5	NS	
Activated	CD19 ⁺ IgM ⁺ IgD ⁺ FSC ^{hi} c	6.2	0.4	6.4	1.1	NS	9.1	1.3	8.9	0.9	NS	9.8	1.1	NS	
MZ	CD19 ⁺ IgM ⁺ IgD ⁻	4.3	0.6	5.1	1.9	NS	6.1	1.2	5.5	1.6	NS	5.7	1.1	NS	
FO	CD19 ⁺ CD21 ⁻ CD23 ⁺	39	3.3	35	5.5	NS	39	3.2	40	3.6	NS	44	4.8	NS	
Spleen															
PBs	CD19 ⁻ B220 ⁺ CD138 ⁺	0.06	0.02	0.13	0.07	0.04	0.19	0.05	0.19	0.04	NS	0.21	0.06	NS	
PCs	CD19 ⁻ B220 ⁻ CD138 ⁺	0.20	0.06	0.37	0.08	0.001	0.39	0.10	0.77	0.20	0.002	0.50	0.13	0.018	
BM															
PBs	CD19 ⁻ B220 ⁺ CD138 ⁺	0.28	0.02	0.42	0.14	0.04	0.40	0.07	0.37	0.10	NS	0.53	0.04	0.004	
PCs	CD19 ⁻ B220 ⁻ CD138 ⁺	0.45	0.008	0.50	0.11	NS	0.44	0.10	0.58	0.20	NS	0.55	0.13	NS	

^aMZ, marginal zone B cells; FO, follicular B cells; PBs, plasmablasts; PCs, plasma cells; BM, bone marrow.

^bData were analyzed using Student's *t* test. *n* = 6 for all genotypes. NS, not significant.

^cFSC^{hi}, high forward scatter.

different fluorophore (Fig. 1B). The KSHV latency locus was active as determined by real-time reverse transcriptase quantitative PCR (RT-qPCR). Since the transgene is only expressed in B cells and whole spleen RNA was used as input, transgene levels were lower than GAPDH (glyceraldehyde 3-phosphate dehydrogenase) levels, but nevertheless consistently detectable. The signal was dependent on reverse transcriptase (RT) (Fig. 1C).

To test the hypothesis that the KSHV latency phenotypes were maintained or perhaps augmented in the BALB/c background, B cell subsets in spleen and bone marrow (BM) were evaluated by flow cytometry (Table 1). KSHV latency mice on the C57BL/6J background exhibit an increased frequency of CD138⁺ plasma cells (PCs). This phenotype was also manifested in the BALB/c background (*P* ≤ 0.05 by Student's *t* test; *n* = 6 per group in comparison to age-matched wild-type mice). In addition to plasma cells (CD19⁻ B220⁻ CD138⁺), the frequencies of plasmablasts (PBs) (CD19⁻ B220⁺ CD138⁺) were increased as well (Fig. 2A and B, F and G, and K). After differentiation in secondary lymphoid organs, the majority of PBs migrate to the BM. The frequencies of PBs, but not the more differentiated PCs, were increased in BM. Note that this represents the steady-state level, as these mice were not specifically immunized to elicit an antibody response. This phenotype is consistent with the notion that KSHV viral miRNAs promote B cell proliferation and differentiation toward the PC stage.

Deletion of the inhibitory receptor FcγRIIB increases PC and PB frequencies in response to antigen stimulation, but only minimally under "normal" conditions. FKO mice had a PB frequency in spleen of 0.19% ± 0.05%, compared to 0.06% ± 0.02% for wild-type mice, and a PC frequency of 0.39% ± 0.10%, compared to 0.20% ± 0.06% for wild-type mice (Table 1). The KSHV latency locus increased the frequency of splenic PCs in the FKO background to 0.77% ± 0.20% (*P* ≤ 0.002 by Student's *t* test with a group size of *n* = 6). The frequencies of splenic PBs and PCs from BM were not significantly changed (Fig. 2C and D, H and I, and K). Abrogation of TLR4 signaling in the latency × FKO background had divergent effects. One the one hand, it reduced the number of PCs in spleen from 0.77% ± 0.20% to 0.50% ± 0.13% (*P* ≤ 0.02 by Student's *t* test with a group size of *n* = 6). On the other hand, it increased the number of PBs in the BM from 0.37% ± 0.10% to 0.53% ± 0.04% (*P* ≤ 0.02 by Student's *t* test with a group size of *n* = 6) (Fig. 2I, J, and K). TLR4-driven PC differentiation is well documented (43–45) and can explain the decreased frequency of splenic PCs in the triple mutant mice. Even though the magnitudes of the effects were small, they are consistent with a model whereby FcγRIIB, TLR4, and KSHV latency genes impact different points in B cell differentiation.

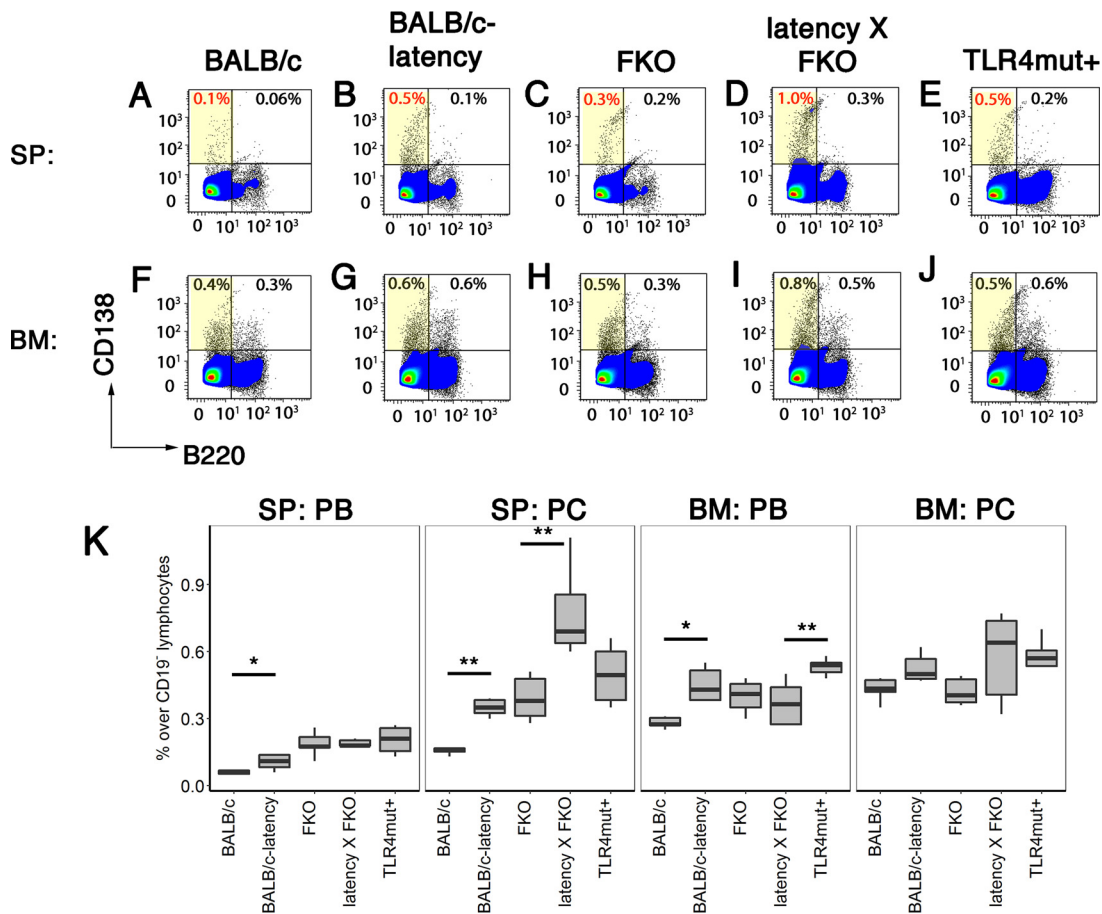


FIG 2 Increased proliferation of PCs in the BALB/c background. Cells were prepared from spleen or BM of BALB/c, BALB/c latency, FKO, latency × FKO, and latency × FKO × TLR4mt+ mice (all n = 6) and analyzed using three-color flow cytometry. CD19⁻ cells were further gated with CD138 and B220. Representative examples of flow diagrams of PBs and PCs are shown in panels A to J. (K) Percentages of PBs (CD19⁻ B220⁺ CD138⁺) and PCs (CD19⁻ B220⁻ CD138⁺) are shown on the vertical axis for each of the mouse genotypes indicated on the horizontal axis. Box plots represent the 1st and 3rd quartiles, with the median indicated by the horizontal line. Whiskers are drawn out to 1.5× the interquartile range. Asterisks indicate significance of pairwise comparison using Tukey's *post hoc* test: *, P ≤ 0.05; **, P ≤ 0.01.

Flow cytometry analysis provides extremely accurate depictions of individual B cell subsets as defined by cell surface markers but does not provide information about spatial organization. Hence, splenic architecture was examined by histology. C57BL/6J-latency mice have a high incidence of lymphoid hyperplasia (LH) in spleen. This phenotype was maintained in the BALB/c latency mice, though only marginally (Table 2). It was augmented in latency × FKO mice compared to FKO mice (P ≤ 0.01 by Fisher's exact test). The frequencies of LH were 17% in FKO mice, 62% in latency × FKO mice, and 58% in latency × FKO × TLR4mut+ mice, i.e., abrogation of TLR4 function did not affect LH incidence. Figure 3 provides representative examples of the different spleen phenotypes observed across mouse genotypes at a young age (13 to 19 weeks).

TABLE 2 Spleen pathology

Phenotype	Rate of spleen pathology in mouse group												
	BALB/c		BALB/c latency		P vs BALB/c ^a	FKO		Latency × FKO		P vs FKO ^a	TLR4mt		P vs latency × FKO ^a
	No. of mice (n = 9)	%	No. of mice (n = 12)	%		No. of mice (n = 24)	%	No. of mice (n = 13)	%		No. of mice (n = 12)	%	
Lymphoid hyperplasia	3	33	9	75	NS	4	17	8	62	0.01	7	58	NS
Normal	6	67	3	25		20	83	5	39		5	42	

^aData were analyzed using Fisher's exact test. A P value of ≤0.05 was regarded as significant. NS, not significant.

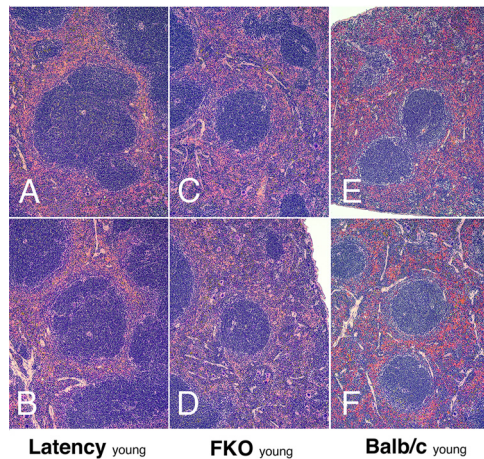


FIG 3 Spleen pathology of young latency \times FKO mice. Representative H&E staining of spleen section is shown for young (13 to 19 weeks of age) latency (A and B), FKO (C and D), and BALB/c (E and F) mice. Magnification, $\times 100$.

Latency mice looked more similar to FKO mice than wild-type BALB/c mice: the primary follicles in the latency and FKO mice showed evidence of hypercellularity (dark center zone) and a loss of the follicular rim zone (Fig. 3E and F) in comparison to wild-type FKO and BALB/c mice. Note, that these are not germinal centers (GCs), as the animals had not been exposed to T-dependent protein antigens. Figure 4 provides representative examples of spleen histology comparing older FKO to latency \times FKO mice (29 to 33 weeks of age). These animals formed the basis for the histological evaluation represented in Table 2. FKO mice maintained the overall architecture into old age, and evidence of follicular hyperplasia waned. The central zones appeared lighter, and a prominent follicular rim zone was apparent in older FKO mice, which is similar to wild-type mice at young age (Fig. 4A and B). In contrast, latency \times FKO mice lost the splenic architecture (Fig. 4C to F) and presented with irregular follicles, many of which were secondary follicles containing GC with prominent light and dark zones. Detailed histology supported the phenotypes as observed by flow cytometry as described above as well as by the functional studies reported below. The histology was consistent with LH, post-GC B cell proliferation, and plasma cell differentiation induced by the KSHV latency transgene and suggests that KSHV latency-induced premalignant hyperplasia was still subject to inhibition by Fc γ R1IB.

KSHV latency locus augments the B cell response to a TD antigen. Enhanced responsiveness to TD and TI antigens is another phenotype of the C57BL/6J latency mice. To test the hypothesis that this phenotype is maintained in the BALB/c background, the degree of *ex vivo* proliferation of purified splenic B lymphocytes was determined by 5-ethynyl-2'-deoxyuridine (EdU) incorporation in response to relevant stimuli. (i) CD40 cross-linking by anti-CD40 antibody mimics T cell stimulation. B cells from FKO mice are deficient in their response to anti-CD40. Compared to the FKO mice, splenic B cells from the latency \times FKO mice displayed higher proliferation to a TD antigen, anti-CD40 ($P = 0.000014$ by analysis of variance [ANOVA] for trend; $n = 5$ per group) (Fig. 5A and B); i.e., KSHV latent genes complemented the FKO defect. The B cells from the TLR4mut $^{+}$ mice were responsive to anti-CD40 (Fig. 5C), though variation within the group was too high for a direct comparison. (ii) LPS is a specific activator of TLR4. FKO and latency \times FKO mice responded similarly to LPS (Fig. 5D to F), while TLR4mut $^{+}$ mice lost the ability to respond ($P = 2.6 \times 10^{-20}$ by ANOVA for trend; $n = 5$ per group). This assay confirms the TLR4 mutant phenotype and establishes that the KSHV latency locus cannot have complemented the TLR4 defect. (iii) All mice responded equally to direct BCR cross-linking by anti-IgM antibody (Fig. 5G and H). This was expected since the inhibitory Fc γ R1IB is not engaged by IgM and TLR activation is dispensable for direct BCR cross-linking via IgM. Taken together, these experiments are

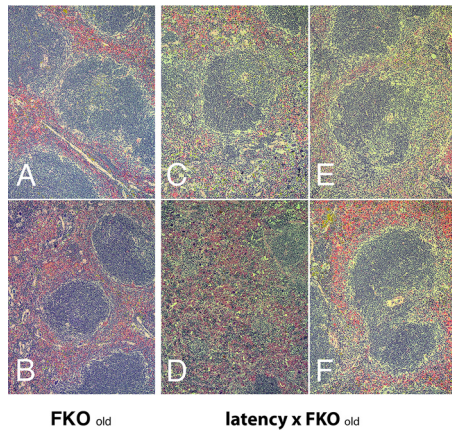


FIG 4 Spleen pathology of old latency × FKO mice. Representative H&E staining of spleen section is shown for old (29 to 33 weeks) FKO (A and B) and latency × FKO (C to F) mice. Magnification, ×100.

consistent with an indirect mechanism by which KSHV latent genes and miRNAs augment the initial events in B cell activation. The viral genes cannot substitute for direct BCR engagement, “signal 1,” in B cell activation or TLR4 activation, but modulate the response and alleviate the dependency on accessory CD4 T-cell-dependent activators such as CD40L, “signal 2.” Such a model would be consistent with the clinical phenotype of KSHV, as MCD and PEL are B cell hyperplasias that develop in HIV-infected, CD4-depleted patients.

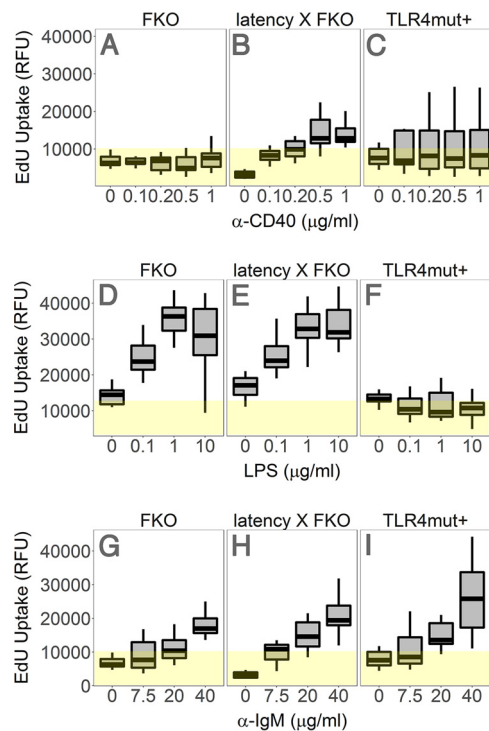


FIG 5 KSHV latency locus-induced hyperresponsiveness to anti-CD40, anti-IgM, and LPS. *Ex vivo* proliferation was assessed by incorporation of 5-ethynyl-2'-deoxyuridine (EdU) into DNA. Splenic B cells from the FKO ($n = 5$), latency × FKO ($n = 5$), and TLR4mut+ ($n = 5$) mice were isolated via negative selection and cultured with various doses of anti-CD40 without IL-4 (A), LPS (B), or anti-IgM (C) for 72 h. EdU uptake is represented as relative fluorescence units (RFU) on the vertical axis. The degree of *ex vivo* proliferation was analyzed by ANOVA. Box plots represent the 1st and 3rd quartiles, with the median indicated by the horizontal line. Whiskers are drawn out to 1.5× the interquartile range. Yellow highlighting represents background signal.

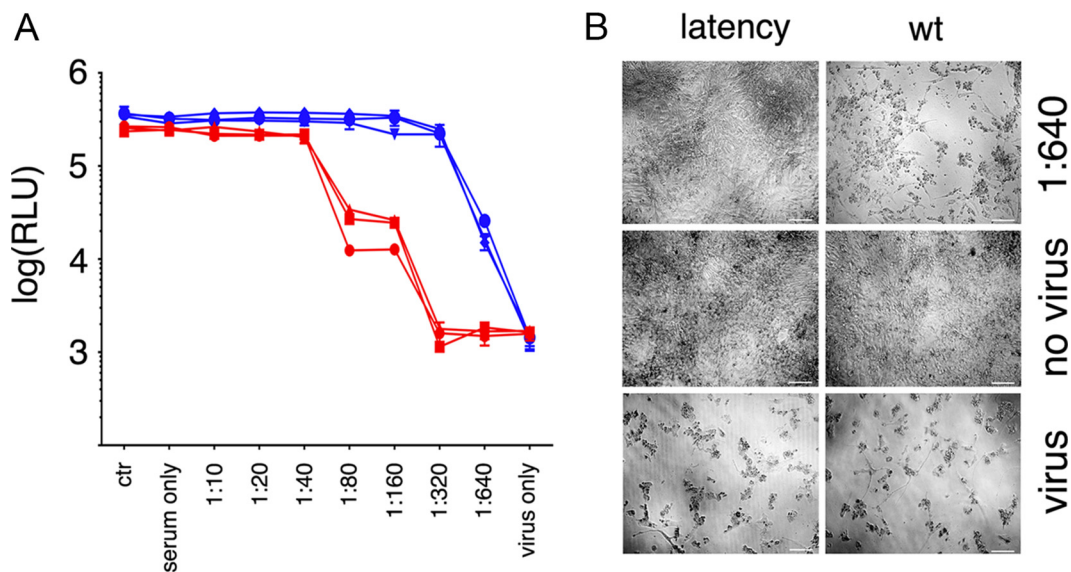


FIG 6 Neutralizing antibody developed to ZIKV in BALB/c latency mice. (A) Vero cell proliferation assay performed by CTG 4 days after diluted serum and Zika virus incubation. Data from $n = 3$ BALB/c mice and $n = 3$ BALB/c latency mice are shown in red and in blue, respectively. The y axis represents relative light units (RLU) from CTG reagent. (B) Representative images from 96-well neutralizing plates. Magnification, $\times 100$. The scale bar represents $100 \mu\text{m}$.

KSHV latency locus augments the antibody response to ZIKV. To verify the response to model stimuli, BALB/c latency mice were infected with the human pathogen ZIKV. ZIKV induces a robust IgG response in immunocompetent humans, nonhuman primates, and mice. BALB/c mice are used as an animal model for infection with ZIKV PRVABC59 (46, 47). The mice rapidly clear the infection and mount a canonical IgG response. Mice were immunized with PRVABC59/alum, and serum was collected 12 days later. Neutralizing antibody titers were determined by endpoint dilution as measured by cell viability (Fig. 6A). Sera of infected wild-type mice ($n = 3$) had a titer of $\sim 1:80$, whereas latency mice ($n = 3$) had a titer of $\sim 1:160$. This demonstrates that antibody production in latency mice is more efficient than in wild-type mice. Figure 6C shows representative images for controls and the highest dilution of serum. These data suggest that latency mice consistently generate higher neutralizing antibody titers in response to viral infection.

Rapamycin ameliorates KSHV latency locus-associated hyperglobulinemia. Polyclonal B cell activation and the ensuing hyperglobulinemia are a common feature of HIV infection. Hyperglobulinemia is also a clinical symptom of human MCD and PEL, which is recapitulated in the KSHV latency mice. Allosteric mTOR inhibitors such as rapamycin are in clinical use to dampen a hyperactive immune response during transplantation and in autoimmunity. To test the hypothesis that mTOR inhibition can curb KSHV-induced, progressive polyclonal B cell activation, we administered everolimus in chow. Steady-state drug levels were verified (Fig. 7A). Treated mice averaged $64 \pm 19 \text{ ng/ml}$ ($n = 5$), which is comparable to concentrations in humans (48). Steady-state levels could be increased ~ 20 -fold to $1,330 \pm 387 \text{ ng/ml}$ ($P \leq 10^{-6}$ by Dunnett's *post hoc* test for ANOVA; $n = 5$ per group) by deleting cytochrome P450 reductase (CYP3A) using HRN nude mice. These mice do not express hepatic CYP3A, which is the key enzyme responsible for biodegradation of rapamycin. Repeated injection of ritonavir, which is part of combination HIV antiretroviral treatment (cART), increased steady-state drug levels ~ 5 -fold to $254 \pm 46 \text{ ng/ml}$ ($P \leq 10^{-6}$ by Dunnett's *post hoc* test for ANOVA by groups; $n = 5$ per group). This was expected as ritonavir is a type of HIV protease inhibitor that inhibits CYP3A biochemically (49). In fact, ritonavir and, more recently, cobicistat are included in all modern cART regimens for their effect on CYP3A, which boosts nonnucleoside reverse transcriptase inhibitor (NNRTI) and nucle-

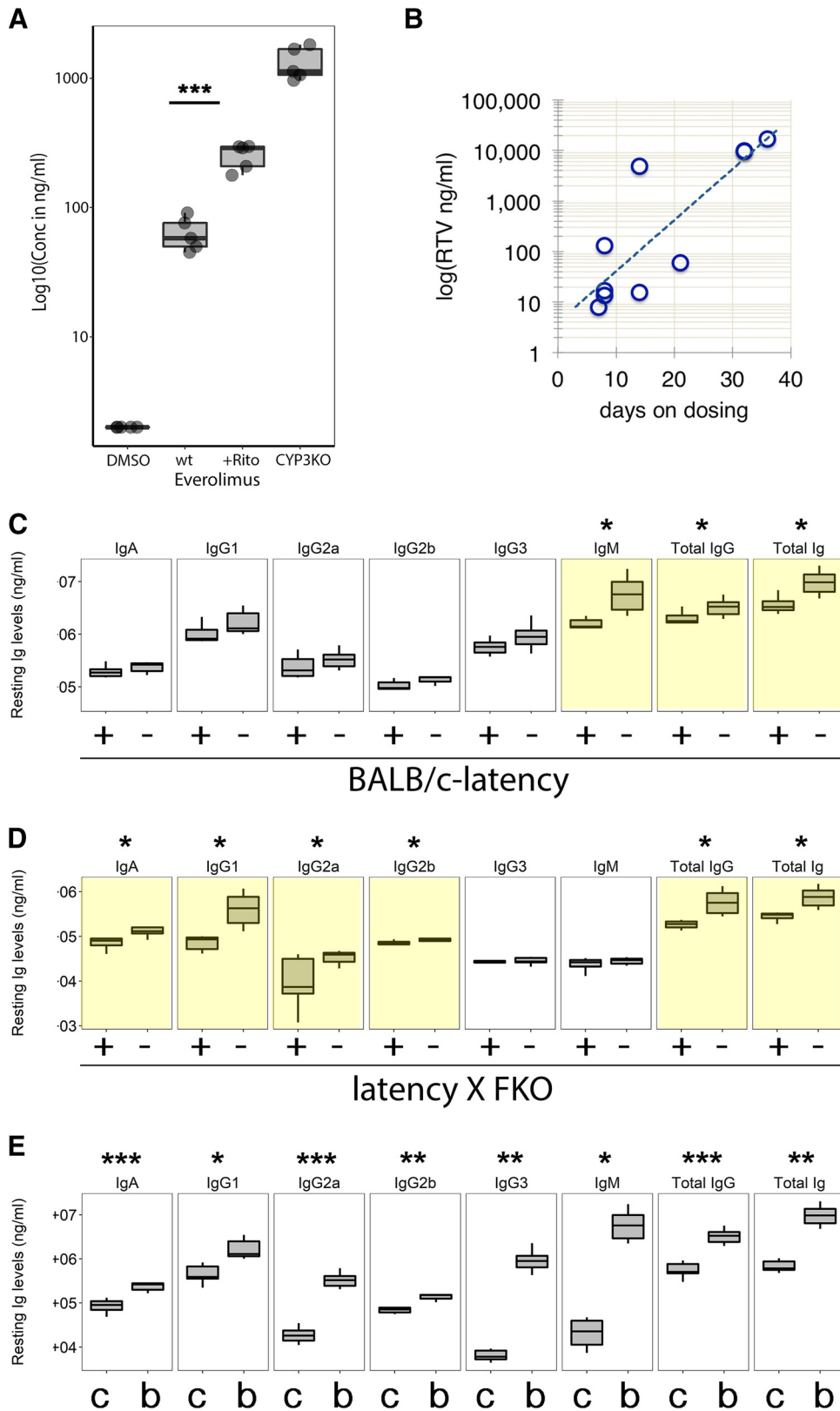


FIG 7 Everolimus dampened KSHV latency-induced hyperglobulinemia polyclonally. (A) Ritonavir-prolonged everolimus level. HRN nude mice were i.p. injected with dimethyl sulfoxide (DMSO [vehicle]) or 3 mg/kg everolimus (CYP3ko) (*n* = 5). NCr nude mice were i.p. injected with 3 mg/kg everolimus (wt) or 3 mg/kg everolimus and 30 mg/kg ritonavir (+Rito) (*n* = 5). The everolimus level was measured from whole blood and plotted. (B) NCr nude mice were i.p. injected with 30 mg/kg ritonavir (RTV) 3 times per week for 2 weeks (*n* = 11). Afterward the level

(Continued on next page)

oside reverse transcriptase inhibitor (NRTI) levels. Figure 7B shows the steady-state ritonavir concentrations that were achieved by 3 injections per week for 2 weeks. These experiments established the drug regimen for long-term treatment with everolimus and show that values for drug metabolism and concentration in mice were comparable to those in humans. Littermates of the latency and latency \times FKO mice were fed with everolimus-containing diet for 3 months. Afterward the levels of resting Ig were determined by isotype-specific enzyme-linked immunosorbent assay (ELISA). First, BALB/c latency mice were evaluated (Fig. 7C). The levels of total Ig and IgG were significantly decreased in mice fed everolimus-containing diet compared to littermate controls fed a regular diet ($P \leq 0.05$ by t test adjusted for multiple comparison by the Bonferroni method; $n = 7$ per group). The level of serum IgM was also reduced. The levels of other individual Ig subtypes were not significantly decreased. Next, BALB/c latency \times FKO mice were evaluated (Fig. 7D). Again, total Ig and IgG levels were significantly ($P \leq 0.05$ by t test adjusted for multiple comparison by the Bonferroni method; $n = 7$ per everolimus and $n = 8$ for regular) decreased in mice fed everolimus-containing diet compared to littermate controls fed a regular diet. Levels of IgA, IgG1, and IgG2a were significantly reduced, while the level of IgM was not. As expected, BALB/c latency mice had significantly increased Ig levels across all isotypes compared to C57BL/6J latency mice (data previously published in reference 19) (Fig. 7E). These experiments establish the ability of rapamycin or its derivatives to reduce KSHV latency locus-dependent hyperglobulinemia in the hypersusceptible BALB/c background.

KSHV latency locus augments pristane-induced inflammation. BALB/cJAn mice (but not BALB/cSc mice) develop intraperitoneal inflammation and plasmacytoma on repeated intraperitoneal pristane injection. To test the hypothesis that the KSHV latency locus augmented inflammatory immune responses in the peritoneum as it did in the spleen, pristane was administered to wild-type, latency, FKO, and latency \times FKO mice. Incidence of intraperitoneal inflammation was monitored over time by measuring ascites formation in the abdominal space. All mice showed chronic intraperitoneal inflammation. Inflammation was identified by counting the number of cells with multilobed nuclei, a defining feature of neutrophils, in ascites (Fig. 8A). The KSHV latency mice had a higher incidence of inflammation around 70 to 150 days postinjection compared to wild-type control mice, consistent with accelerated disease onset. None of the mice died, and the experiment was continued until all mice showed disease (Fig. 8B). Disease acceleration became more pronounced in FKO mice (Fig. 8C). Latency \times FKO mice consistently exhibited higher inflammation than FKO mice ($P \leq 0.01$ by log rank test; group sizes of $n = 35$ for FKO mice and $n = 24$ for latency \times FKO mice). We did not observe an association with sex. In sum, disease progression in response to pristane was accelerated by the KSHV latency genes.

DISCUSSION

KSHV is a lymphotropic herpesvirus that establishes latency in B cells and silently persists for many years prior to disease manifestation (reviewed in reference 50). Hence, understanding KSHV's interaction with B cells is central to understanding the biology of this virus. During latency, a limited set of viral genes are expressed: these include the LANA, vCYC, and vFLIP genes and all viral miRNAs. Notably, KSHV miR-K12-11 is an ortholog of human and murine mir-155, with sequence identity across all three variants

FIG 7 Legend (Continued)

of ritonavir was measured. (C) Levels of Igs were measured using isotype-specific ELISA and plotted from mice fed everolimus-containing diet (+) and those fed regular diet (-). For BALB/c latency mice, $n = 7$ for both the everolimus and regular diet groups. (D) Levels of Igs were measured using isotype-specific ELISA and plotted from mice fed everolimus-containing diet and those fed regular diet. For latency \times FKO mice, $n = 7$ for the everolimus diet group and $n = 8$ for the regular diet group. (E) Comparison of Ig levels from the C57BL/6J latency (c) and BALB/c latency (b) mice. This represents a meta-analysis. Ig levels from C57BL/6J latency mice were previously reported (19). Box plots represent the 1st and 3rd quartiles, with the median indicated by the horizontal line. Whiskers are drawn out to $1.5\times$ the interquartile range. Asterisks indicate significant difference by ANOVA: *, $P \leq 0.05$; **, $P \leq 0.005$; ***, $P \leq 0.0005$.

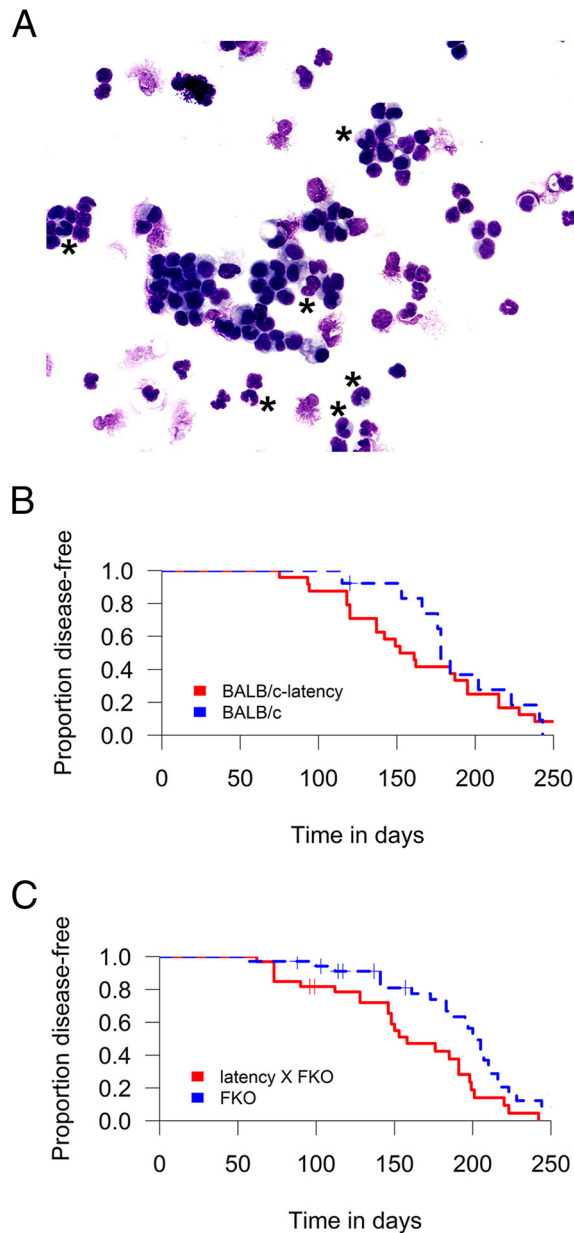


FIG 8 Augmented incidence of pristane-induced inflammation. (A) Representative image of ascites. Inflammation is exemplified by a high number of neutrophils found in a BALB/c latency mouse at day 137 postinjection of pristane. Asterisks indicate neutrophils. Giemsa stain. Magnification, $\times 400$. (B and C) Disease-free plot of pristane-injected mice. The x axis represents days postinjection. The log-rank test was used to analyze for BALB/c and BALB/c latency mice in panel B and for FKO and FKO \times latency mice in panel C.

extending past the seed region and with all variants exhibiting similar biological activities (22, 51–53). This report establishes that KSHV latency-dependent B cell phenotypes are augmented in the BALB/c background. BALB/c mice are the preferred model to develop monoclonal antibodies, to study B cell development, and to study polyclonal B cell activation events that underlie autoimmunity (54, 55). In comparison to C57BL/6 mice, the B cell response to antigen in BALB/c mice is more pronounced and thus allows for more detailed immunological investigations. BALB/c latency mice thus represent a novel animal model to study KSHV-associated B cell reprogramming.

We hypothesized that deletion of $Fc\gamma RIIB$ would enhance KSHV latency-induced immune pathogenesis. $Fc\gamma RIIB$ is the only $Fc\gamma$ receptor expressed on B cells. It is a

cell-autonomous inhibitory receptor that curbs plasma cell proliferation after antigen exposure has subsided (reviewed in reference 32). It fulfilled the same function in KSHV latency locus-driven phenotypes. Plasma cell frequency, lymphoid hyperplasia, and gross disorganization of the spleen in aged mice were increased in latency \times Fc γ RIIB-deleted mice. Latency \times Fc γ RIIB-deleted mice showed enhanced responses to CD40 stimulation in culture compared to Fc γ RIIB-deleted mice. This seemed counterintuitive, as the initial characterization of Fc γ RIIB-deleted mice suggested the opposite (33). More recent reports, however, have uncovered an additional function for Fc γ RIIB in supporting the immune-stimulatory function of anti-CD40 on B cells (34, 56, 57) and have shown that Fc γ RIIB-deficient mice are defective in responding to CD40L. The KSHV latency genes complemented this deficiency, just as they complemented IL-6 and mir-155 deficiency under conditions of low antigen load. The immune-stimulatory function of the KSHV latency locus extended to natural infection with ZIKV. These observations support the notion that KSHV latency genes act at the initiation stage of the B cell activation, perhaps by lowering the BCR activation threshold and/or exaggerating the progrowth signals of CD40-CD40L interaction.

There is an immediate practical application of these findings. We expect that BALB/c latency mice are better at inducing Ig responses to adjuvanted antigens than BALB/c or BALB/c FKO mice. Anti-CD40 has been explored as a potent adjuvant in vaccine design (58, 59). For instance, a vaccine against lymphoma consisting of an anti-CD40 antibody chemically coupled to the tumor idiotype, A20, inhibited tumor growth in a mouse lymphoma model (60). Pristane is the active component in Freund's incomplete adjuvant (61), and BALB/c latency \times FKO mice responded better than FKO mice alone. These observations allude to the potential utility of BALB/c latency mice for high-efficiency monoclonal antibody development.

Hyperglobulinemia in BALB/c latency \times FKO mice and BALB/c latency mice was ameliorated by long-term, continuous dosing with the allosteric mTOR inhibitor everolimus. The same dosing regimen was also associated with extending overall life span in mammals, by systemically reducing glycolysis (62). It mimics the clinical regimen and target trough levels in solid organ transplantation, in the treatment of autoimmune diseases (63, 64), and in stabilizing disease progression in KS (36, 48, 65). Further studies are needed, particularly as to the interaction with proteinase inhibitors or other boosters used in advanced cART, such as cobicistat. Overall the experiments presented here support the idea of using rapamycin to limit polyclonal B cell activation in KSHV-associated disease such as MCD, KSHV inflammatory cytokine syndrome, KS-associated immune reconstitution inflammatory syndrome, or perhaps even in HIV-associated, LPS/TLR4-driven immune activation (2, 66, 67).

In sum, this new mouse model resembles the premalignant conditions of KSHV infection, such as MCD as well as subclinical immune activation associated with primary KSHV infection and latency (68, 69). The majority of HIV- and KSHV-coinfected persons live in a state of constant, low-level B cell activation unless cART failure or failure to access cART causes progression to full-blown AIDS. In sub-Saharan Africa, KSHV infection happens early in life (70). Here, KS is a disease of (i) children, (ii) the elderly, and (iii) people of all ages coinfecting with HIV. Coinfections with parasites, such as the malaria parasite, are common. We do not know how these multiple pathogens, rhadinoviruses, and other infections (71–73), as well as since the late 1950's HIV-1, interact or how these interactions would change in response to vaccination. BALB/c KSHV latency mice provide a first, albeit extremely reductionist, model to investigate the immune response to pathogens secondary to KSHV infection.

MATERIALS AND METHODS

Mice. Transgenic mice that express the KSHV latency locus were previously described (19). The background of the original latency mice was C57BL/6J, and mice were crossed into the BALB/cByJ background for 10 generations. Latency mice in the BALB/c background (BALB/c latency) were further crossed with BALB/c Fc γ RIIB knockout mice [FKO; C.129S4(B6)-Fcgr2b^{tm1Ttk}/cAnNTac N12], which were obtained from Taconic (Hudson, NY) (33). These mice (latency \times FKO) were further crossed into BALB/c-TLR4 mutant mice (C.C3-Tlr4^{Lps-d/J}) from the Jackson Lab (Bar Harbor, ME) to generate the latency

mice, which do not express the Fc γ receptor IIB and show a defective response to LPS (referred to as TLR4mut+) (28, 29). All mice were maintained under pathogen-free conditions using ventilated cages. All experiments were approved by the Institutional Animal Care and Use Committee (IACUC) at the University of North Carolina at Chapel Hill (UNC).

Genotyping and transgene expression. Genomic DNA was isolated from mouse tail clipping using a Wizard SV genomic DNA kit (Promega). qPCR was performed for LANA and ApoB primers as previously described (74). Mice without Fc γ receptor IIB were typed by PCR as previously described (33). TLR4 mutant mice were genotyped according to the supplier's protocol. To evaluate gene expression, total RNA from spleen was isolated and reverse transcribed, and gene expression was quantitated by real-time qPCR. An RT-negative reaction mixture was included with each sample. Positive samples were 5 threshold cycle (C_T) units, or $\sim 2^5 = 32$ -fold above the limit of detection of the assay, which was set at 40 cycles. At $C_T = 40$, no product was generated, as ascertained by gel electrophoresis of the reaction. Murine GAPDH was used as a positive control.

Pathology evaluation. Extraction of spleen and femur and initial gross examination were performed at the time of sacrifice or death. Tissues were embedded in paraffin, sectioned, and stained with hematoxylin and eosin (H&E) at the Animal Histopathology Core facility of the UNC Lineberger Comprehensive Cancer Center (LCCC). Pathological diagnosis was performed by a veterinary pathologist (Y. Kim) based on H&E staining. A microscope (Nikon Eclipse Ci Y-TV55; Nikon, Japan) was used for all pathological evaluation. Images were captured using a camera (Jenoptik ProgRes SpeedXT core 3; Jenoptik, Germany) and acquired using ProgRes CapturePro (version 2.8; Jenoptik). The magnifications of the objective lenses were $\times 2$, $\times 10$, or $\times 40$.

Flow cytometry. Flow cytometry analysis was carried out as previously reported (74). Briefly, cells were purified from the spleen or bone marrow in 7- to 11-week-old mice. One million cells were stained after red blood cell lysis. The following antibodies were used: allophycocyanin-conjugated anti-mouse CD19 (clone 6D5), anti-mouse CD23 (clone B3B4), and fluorescein isothiocyanate (FITC)-conjugated anti-mouse CD45R (clone RA3-6B2) from Invitrogen and FITC-conjugated anti-mouse IgD (clone 11-26c.2a), phycoerythrin-conjugated anti-mouse CD138 (clone 281-2), anti-mouse CD21/CD35 (clone 7G6), and anti-mouse IgM (clone R6-60.2) from BD Biosciences. Data were acquired using a CyAn instrument (Beckman Coulter) at the UNC Flow Cytometry Core and analyzed using Flowjo version 7.6.5 (Tree Star, Inc.).

ZIKV infection studies. BALB/c latency and BALB/cByJ mice at ages 6 to 8 weeks were infected via i.p. injection of 10^7 PFU ZIKV strain PRVABC59 at a 1:1 final volume with an adjuvant (Imject alum; Thermo Scientific). Serum was isolated from infected mouse 12 days postinjection and was stored at -80°C until further analysis. All experiments were performed under biosafety level 2 (A-BSL2) containment.

Neutralization assay. Vero cells were maintained in Dulbecco's modified Eagle's medium (DMEM) containing 100 units of penicillin G, 100 $\mu\text{g}/\text{ml}$ streptomycin, and 2 mM L-glutamine (complete DMEM). Serum samples were serially diluted 1:2 in a 96-well plate by a Freedom EVO 100 robot (Tecan), and ZIKV PR at a multiplicity of infection (MOI) of 1 was added in each well. After 1 h of incubation at 37°C , this mixture was transferred to 96-well plate containing a confluent monolayer of Vero cells. After 2 days of incubation, supernatants were replaced with the complete DMEM; after another 2 days, pictures of each well were collected by Leica DMIL microscope and AxioCam ERc5s camera (Zeiss) with a $\times 10$ magnification, and cell proliferation was measured by a CellTiter-Glo (CTG) luminescence cell viability assay (Promega) (75), adding the reagent for 10 min at room temperature and reading the luminescence by a FLUORstar Optima microplate reader (BMG Labtech).

Immunofluorescence assay. The Vero cells used in the neutralization assay were fixed in 4% paraformaldehyde for 20 min, washed with phosphate-buffered saline (PBS), and permeabilized and blocked with 10% goat serum and 0.2% Triton X-100 in PBS for 1 h; subsequently, cells were stained with 1:100 mouse anti-flavivirus E-glycoprotein antibody (clone 3571; Abcam) overnight. The next day, cells were washed with TTBS (100 mM Tris-HCl, 0.9% NaCl, 0.1% Tween 20, pH 7.5), incubated for 1 h in the dark with anti-mouse Texas Red-conjugated secondary antibody (1:500; Vector Laboratories), and washed again with TTBS, and the slides were mounted with Prolong Gold antifade (Cell Signaling). Images were acquired by a Leica DM4000B epifluorescence microscope and QImaging Retiga 2000RV camera at a $\times 100$ magnification.

Flow cytometry. Flow cytometry analysis was carried out as previously reported (74). Briefly, cells were purified from the spleen or bone marrow in 7- to 11-week-old mice. One million cells were stained after red blood cell lysis. Data were acquired using a CyAn instrument (Beckman Coulter) at the UNC Flow core and analyzed using Flowjo version 7.6.5 (Tree Star, Inc.).

Ex vivo B-cell proliferation assay. Splenic B cells were isolated from 8- to 11-week-old FKO, latency \times FKO, or TLR4mt+ mice (all $n = 5$) using an EasySep mouse B cell enrichment kit (StemCell Technologies). B cells were cultured in RPMI 1640 medium supplemented with 20% fetal bovine serum, 2 mM L-glutamine, penicillin (0.05 $\mu\text{g}/\text{ml}$), streptomycin (5 U/ml), and 0.1% β -mercaptoethanol (vol/vol) (Invitrogen) with anti-CD40 MAb (clone HM40-3; Biolegend), F(ab') $_2$ goat anti-mouse IgM antibody (Jackson ImmunoResearch Laboratory), or LPS (from *Escherichia coli* 0111:B4; InvivoGen) at 37°C under 5% CO_2 . The *ex vivo* proliferation was assessed using a Click-iT Edu microplate assay kit (Invitrogen) according to the supplier's manual.

Everolimus diet experiment. NCr nude (CrTac:NCr-Foxn1^{nu}) and HRN nude [NCr-Por^{tm1Wolf} Foxn1^{nu} Tg(Alb-cre)21Mgn] mice were obtained from Taconic (Hudson, NY). Everolimus (3 mg/kg) and ritonavir (3 mg/kg) were intraperitoneally (i.p.) administered to these nude mice for 8 months. The level of everolimus was measured from whole blood by high-performance liquid chromatography-tandem mass spectrometry (sensitivity of 2 to 50 ng/ml). The BALB/c latency and the latency \times FKO mice were fed with

a diet containing 30 ppm everolimus (Envigo, WI) or control diet (Envigo 2920X) for 3 months. Ritonavir (30 mg/kg) was administered i.p. for the last 2 weeks (on Monday and Thursday each week). Ritonavir levels were measured at the UNC Center for AIDS Research Clinical Pharmacology Core. Serum was collected from mice, and Ig levels were measured as previously described (19).

Pristane experiment. Pristane (2,6,10,14-tetramethylpentadecane) was obtained from Sigma (St. Louis, MO). Five hundred microliters of pristane was injected i.p. into BALB/c, BALB/c latency, FKO, and latency × FKO mice (3 to 4 months old) three times at 2-month intervals. Mice were monitored for 8 months after injection and euthanized when found moribund. Spleen and liver were extracted and embedded in paraffin for pathological evaluation. Cells were prepared from intraperitoneal ascites and gently deposited onto microscopic slides using a cytocentrifuge (StatSpin Cytofuge 12; Beckman Coulter). Then the slides were stained with Giemsa (ScyTek).

Statistical analysis. Data are presented as mean ± standard deviation (SD). Continuous data were analyzed with ANOVA and adjusted for multiple comparisons by Dunnett's method or Tukey's *post hoc* test using R version 3.1.1 (2014-07-10). Incidence data were analyzed with Student's *t* test or Fisher's exact test. A *P* value of ≤0.05 was regarded as statistically significant.

Ethics statement. All animal work was approved by the IACUC of The University of North Carolina at Chapel Hill under 13-219.0/KSHV latency mice. All work has been conducted in accordance with *Public Health Service Policy on Humane Care and Use of Laboratory Animals* (National Institutes of Health, Bethesda, MD), the Amended Animal Welfare Act of 1985, and the regulations of the United States Department of Agriculture (USDA).

ACKNOWLEDGMENTS

We thank Blossom Damania for critical readings and helpful discussions and Helen Lazear for providing ZIKV PRVABC59 seed stock.

The UNC LCCC Animal Histopathology Core is supported in part by an NCI Center Core Support grant (5P30CA016086-41) to the UNC LCCC. The LCCC Animal Studies Core is supported in part by an NCI Center Core Support grant (CA16086) to the UNC Lineberger Comprehensive Cancer Center. The UNC Flow Cytometry Core Facility is supported in part by an NCI Center Core Support grant (P30 CA016086) to the UNC LCCC. D.P.D. and S.H.S. received support from NIH Public Health Service grants P01 CA019014 and R01 DE018304.

REFERENCES

1. Feinstein AR, Petersdorf RG. 1956. The clinical significance of hyperglobulinemia. I. Diagnostic implications. *Ann Intern Med* 44:899–924.
2. Fajgenbaum DC, Uldrick TS, Bagg A, Frank D, Wu D, Srkalovic G, Simpson D, Liu AY, Menke D, Chandrakasan S, Lechowicz MJ, Wong RS, Pierson S, Paessler M, Rossi JF, Ide M, Ruth J, Croglio M, Suarez A, Krymskaya V, Chadburn A, Colleoni G, Nasta S, Jayanthan R, Nabel CS, Casper C, Dispenzieri A, Fosså A, Kelleher D, Kurzrock R, Voorhees P, Dogan A, Yoshizaki K, van Rhee F, Oksenhendler E, Jaffe ES, Elenitoba-Johnson KS, Lim MS. 2017. International, evidence-based consensus diagnostic criteria for HHV-8-negative/idiopathic multicentric Castlemans disease. *Blood* 129:1646–1657. <https://doi.org/10.1182/blood-2016-10-746933>.
3. Wu SJ, Hung CC, Chen CH, Tien HF. 2009. Primary effusion lymphoma in three patients with chronic hepatitis B infection. *J Clin Virol* 44:81–83. <https://doi.org/10.1016/j.jcv.2008.08.015>.
4. Cesarman E, Chang Y, Moore PS, Said JW, Knowles DM. 1995. Kaposi's sarcoma-associated herpesvirus-like DNA sequences in AIDS-related body-cavity-based lymphomas. *N Engl J Med* 332:1186–1191. <https://doi.org/10.1056/NEJM199505043321802>.
5. Soulier J, Grollet L, Oksenhendler E, Cacoub P, Cazals-Hatem D, Babinet P, d'Agay MF, Clauvel JP, Raphael M, Degos L, Sigaux F. 1995. Kaposi's sarcoma-associated herpesvirus-like DNA sequences in multicentric Castlemans's disease. *Blood* 86:1276–1280.
6. Bergquam EP, Avery N, Shiigi SM, Axthelm MK, Wong SW. 1999. Rhesus rhadinovirus establishes a latent infection in B lymphocytes in vivo. *J Virol* 73:7874–7876.
7. Damania B, DeMaria M, Jung JU, Desrosiers RC. 2000. Activation of lymphocyte signaling by the R1 protein of rhesus monkey rhadinovirus. *J Virol* 74:2721–2730. <https://doi.org/10.1128/JVI.74.6.2721-2730.2000>.
8. Salinas E, Gupta A, Sifford JM, Oldenburg DG, White DW, Forrest JC. 2018. Conditional mutagenesis in vivo reveals cell type- and infection stage-specific requirements for LANA in chronic MHV68 infection. *PLoS Pathog* 14:e1006865. <https://doi.org/10.1371/journal.ppat.1006865>.
9. Terrell S, Speck SH. 2017. Murine gammaherpesvirus M2 antigen modulates splenic B cell activation and terminal differentiation in vivo. *PLoS Pathog* 13:e1006543. <https://doi.org/10.1371/journal.ppat.1006543>.
10. Reddy SS, Foreman HC, Sioux TO, Park GH, Poli V, Reich NC, Krug LT. 2016. Ablation of STAT3 in the B cell compartment restricts gammaherpesvirus latency in vivo. *mBio* 7:e00723-16. <https://doi.org/10.1128/mBio.00723-16>.
11. Coleman CB, McGraw JE, Feldman ER, Roth AN, Keyes LR, Grau KR, Cochran SL, Waldschmidt TJ, Liang C, Forrest JC, Tibbetts SA. 2014. A gammaherpesvirus Bcl-2 ortholog blocks B cell receptor-mediated apoptosis and promotes the survival of developing B cells in vivo. *PLoS Pathog* 10:e1003916. <https://doi.org/10.1371/journal.ppat.1003916>.
12. Rekow MM, Darrah EJ, Mboko WP, Lange PT, Tarakanova VL. 2016. Gammaherpesvirus targets peritoneal B-1 B cells for long-term latency. *Virology* 492:140–144. <https://doi.org/10.1016/j.virol.2016.02.022>.
13. Getahun A, Wemlinger SM, Rudra P, Santiago ML, van Dyk LF, Cambier JC. 2017. Impaired B cell function during viral infections due to PTEN-mediated inhibition of the PI3K pathway. *J Exp Med* 214:931–941. <https://doi.org/10.1084/jem.20160972>.
14. Fakhari FD, Jeong JH, Kanan Y, Dittmer DP. 2006. The latency-associated nuclear antigen of Kaposi sarcoma-associated herpesvirus induces B cell hyperplasia and lymphoma. *J Clin Invest* 116:735–742. <https://doi.org/10.1172/JCI26190>.
15. Anders PM, Montgomery ND, Montgomery SA, Bhatt AP, Dittmer DP, Damania B. 2018. Human herpesvirus-encoded kinase induces B cell lymphomas in vivo. *J Clin Invest* 128:2519–2534. <https://doi.org/10.1172/JCI97053>.
16. Ballon G, Akar G, Cesarman E. 2015. Systemic expression of Kaposi sarcoma herpesvirus (KSHV) Vflap in endothelial cells leads to a profound proinflammatory phenotype and myeloid lineage remodeling in vivo. *PLoS Pathog* 11:e1004581. <https://doi.org/10.1371/journal.ppat.1004581>.
17. Sodhi A, Chaisuparat R, Hu J, Ramsdell AK, Manning BD, Sausville EA, Sawai ET, Molinolo A, Gutkind JS, Montaner S. 2006. The TSC2/mTOR pathway drives endothelial cell transformation induced by the Kaposi's

- sarcoma-associated herpesvirus G protein-coupled receptor. *Cancer Cell* 10:133–143. <https://doi.org/10.1016/j.ccr.2006.05.026>.
18. Jeong JH, Hines-Boyd R, Ash JD, Dittmer DP. 2002. Tissue specificity of the Kaposi's sarcoma-associated herpesvirus latent nuclear antigen (LANA/orf73) promoter in transgenic mice. *J Virol* 76:11024–11032. <https://doi.org/10.1128/JVI.76.21.11024-11032.2002>.
 19. Sin SH, Dittmer DP. 2013. Viral latency locus augments B-cell response in vivo to induce chronic marginal zone enlargement, plasma cell hyperplasia, and lymphoma. *Blood* 121:2952–2963. <https://doi.org/10.1182/blood-2012-03-415620>.
 20. Sin SH, Kim Y, Eason A, Dittmer DP. 2015. KSHV latency locus cooperates with Myc to drive lymphoma in mice. *PLoS Pathog* 11:e1005135. <https://doi.org/10.1371/journal.ppat.1005135>.
 21. Sin SH, Kang SA, Kim Y, Eason A, Tan K, An H, Dittmer DP. 2016. Kaposi's sarcoma-associated herpesvirus latency locus compensates for interleukin-6 in initial B cell activation. *J Virol* 90:2150–2154. <https://doi.org/10.1128/JVI.02456-15>.
 22. Sin SH, Kim YB, Dittmer DP. 2013. Latency locus complements microRNA 155 deficiency in vivo. *J Virol* 87:11908–11911. <https://doi.org/10.1128/JVI.01620-13>.
 23. Yoshiki A, Moriwaki K. 2006. Mouse phenome research: implications of genetic background. *ILAR J* 47:94–102. <https://doi.org/10.1093/ilar.47.2.94>.
 24. Anderson PN, Potter M. 1969. Induction of plasma cell tumours in BALB-c mice with 2,6,10,14-tetramethylpentadecane (pristane). *Nature* 222:994–995. <https://doi.org/10.1038/222994a0>.
 25. Kovalchuk AL, Kim JS, Park SS, Coleman AE, Ward JM, Morse HC, Kishimoto T, Potter M, Janz S. 2002. IL-6 transgenic mouse model for extraosseous plasmacytoma. *Proc Natl Acad Sci U S A* 99:1509–1514. <https://doi.org/10.1073/pnas.022643999>.
 26. Zhang S, Ramsay ES, Mock BA. 1998. Cdkn2a, the cyclin-dependent kinase inhibitor encoding p16INK4a and p19ARF, is a candidate for the plasmacytoma susceptibility locus, Pctrl. *Proc Natl Acad Sci U S A* 95:2429–2434. <https://doi.org/10.1073/pnas.95.5.2429>.
 27. Suematsu S, Matsuda T, Aozasa K, Akira S, Nakano N, Ohno S, Miyazaki J, Yamamura K, Hirano T, Kishimoto T. 1989. IgG1 plasmacytosis in interleukin 6 transgenic mice. *Proc Natl Acad Sci U S A* 86:7547–7551. <https://doi.org/10.1073/pnas.86.19.7547>.
 28. Poltorak A, He X, Smirnova I, Liu M-Y, Huffer CV, Du X, Birdwell D, Alejos E, Silva M, Galanos C, Freudenberg M, Ricciardi-Castagnoli P, Layton B, Beutler B. 1998. Defective LPS signaling in C3H/HeJ and C57BL/10ScCr mice: mutations in Tlr4 gene. *Science* 282:2085–2088. <https://doi.org/10.1126/science.282.5396.2085>.
 29. Vogel SN, Johnson D, Perera P-Y, Medvedev A, Larivière L, Qureshi ST, Malo D. 1999. Cutting edge: functional characterization of the effect of the C3H/HeJ defect in mice that lack an Lpsn gene: in vivo evidence for a dominant negative mutation. *J Immunol* 162:5666–5670.
 30. Vogel SN, Wax JS, Perera PY, Padlan C, Potter M, Mock BA. 1994. Construction of a BALB/c congenic mouse, CC3H-Lpsd, that expresses the Lpsd allele: analysis of chromosome 4 markers surrounding the Lps gene. *Infect Immun* 62:4454–4459.
 31. Nimmerjahn F, Ravetch JV. 2008. Fc[gamma] receptors as regulators of immune responses. *Nat Rev Immunol* 8:34–47. <https://doi.org/10.1038/nri2206>.
 32. White AL, Beers SA, Cragg MS. 2014. Fc gamma R1B as a key determinant of agonistic antibody efficacy. *Curr Top Microbiol Immunol* 382:355–372. https://doi.org/10.1007/978-3-319-07911-0_16.
 33. Takai T, Ono M, Hikida M, Ohmori H, Ravetch JV. 1996. Augmented humoral and anaphylactic responses in Fc gamma RII-deficient mice. *Nature* 379:346–349. <https://doi.org/10.1038/379346a0>.
 34. Li F, Smith P, Ravetch JV. 2014. Inhibitory Fcγ receptor is required for the maintenance of tolerance through distinct mechanisms. *J Immunol* 192:3021–3028. <https://doi.org/10.4049/jimmunol.1302934>.
 35. Riva G, Luppi M, Barozzi P, Forghieri F, Potenza L. 2012. How I treat HHV8/KSHV-related diseases in posttransplant patients. *Blood* 120:4150–4159. <https://doi.org/10.1182/blood-2012-04-421412>.
 36. Sin SH, Roy D, Wang L, Staudt MR, Fakhari FD, Patel DD, Henry D, Harrington WJ, Jr, Damania BA, Dittmer DP. 2007. Rapamycin is efficacious against primary effusion lymphoma (PEL) cell lines in vivo by inhibiting autocrine signaling. *Blood* 109:2165–2173. <https://doi.org/10.1182/blood-2006-06-028092>.
 37. Stallone G, Schena A, Infante B, Di Paolo S, Loverre A, Maggio G, Ranieri E, Gesualdo L, Schena FP, Grandaliano G. 2005. Sirolimus for Kaposi's sarcoma in renal-transplant recipients. *N Engl J Med* 352:1317–1323. <https://doi.org/10.1056/NEJMoa042831>.
 38. Fernandez D, Bonilla E, Mirza N, Niland B, Perl A. 2006. Rapamycin reduces disease activity and normalizes T cell activation-induced calcium fluxing in patients with systemic lupus erythematosus. *Arthritis Rheum* 54:2983–2988. <https://doi.org/10.1002/art.22085>.
 39. Prevel N, Allenbach Y, Klatzmann D, Salomon B, Benveniste O. 2013. Beneficial role of rapamycin in experimental autoimmune myositis. *PLoS One* 8:e74450. <https://doi.org/10.1371/journal.pone.0074450>.
 40. Stylianou K, Petrakis I, Mavroei V, Stratakis S, Vardaki E, Perakis K, Stratigis S, Passam A, Papadogiorgaki E, Giannakakis K, Nakopoulou L, Daphnis E. 2011. The PI3K/Akt/mTOR pathway is activated in murine lupus nephritis and downregulated by rapamycin. *Nephrol Dial Transplant* 26:498–508. <https://doi.org/10.1093/ndt/gfq496>.
 41. O'Reilly T, McSheehy PM, Kawai R, Kretz O, McMahon L, Brueggen J, Bruelisauer A, Gschwind HP, Allegrini PR, Lane HA. 2010. Comparative pharmacokinetics of RAD001 (everolimus) in normal and tumor-bearing rodents. *Cancer Chemother Pharmacol* 65:625–639. <https://doi.org/10.1007/s00280-009-1068-8>.
 42. O'Donnell A, Faivre S, Burris HA, III, Rea D, Papadimitrakopoulou V, Shand N, Lane HA, Hazell K, Zoellner U, Kovarik JM, Brock C, Jones S, Raymond E, Judson I. 2008. Phase I pharmacokinetic and pharmacodynamic study of the oral mammalian target of rapamycin inhibitor everolimus in patients with advanced solid tumors. *J Clin Oncol* 26:1588–1595. <https://doi.org/10.1200/JCO.2007.14.0988>.
 43. Anderson J, Sjöberg O, Moller G. 1972. Induction of immunoglobulin and antibody synthesis in vitro by lipopolysaccharides. *Eur J Immunol* 2:349–353. <https://doi.org/10.1002/eji.1830020410>.
 44. Coutinho A, Gronowicz E, Bullock WW, Möller G. 1974. Mechanism of thymus-independent immunocyte triggering. *J Exp Med* 139:74–92. <https://doi.org/10.1084/jem.139.1.74>.
 45. Goodnow CC, Brink R, Adams E. 1991. Breakdown of self-tolerance in anergic B lymphocytes. *Nature* 352:532–536. <https://doi.org/10.1038/352532a0>.
 46. Chan JF-W, Zhang AJ, Chan CC-S, Yip CC-Y, Mak WW-N, Zhu H, Poon VK-M, Tee K-M, Zhu Z, Cai J-P, Tsang JO-L, Chik KK-H, Yin F, Chan K-H, Kok K-H, Jin D-Y, Au-Yeung RK-H, Yuen K-Y. 2016. Zika virus infection in dexamethasone-immunosuppressed mice demonstrating disseminated infection with multi-organ involvement including orchitis effectively treated by recombinant type I interferons. *EBioMedicine* 14:112–122. <https://doi.org/10.1016/j.ebiom.2016.11.017>.
 47. Larocca RA, Abbink P, Peron JPS, de Zanotto APM, Iampietro MJ, Badamchi-Zadeh A, Boyd M, Ng'anga D, Kirilova M, Nityanandam R, Mercado NB, Li Z, Moseley ET, Bricault CA, Borducchi EN, Giglio PB, Jetton D, Neubauer G, Nkolola JP, Maxfield LF, De La Barrera RA, Jarman RG, Eckels KH, Michael NL, Thomas SJ, Barouch DH. 2016. Vaccine protection against Zika virus from Brazil. *Nature* 536:474. <https://doi.org/10.1038/nature18952>.
 48. Krown SE, Roy D, Lee JY, Dezube BJ, Reid EG, Venkataramanan R, Han K, Cesarman E, Dittmer DP. 2012. Rapamycin with antiretroviral therapy in AIDS-associated Kaposi sarcoma: an AIDS Malignancy Consortium study. *J Acquir Immune Defic Syndr* 59:447–454. <https://doi.org/10.1097/QAI.0b013e31823e7884>.
 49. Knox TA, Oleson L, von Moltke LL, Kaufman RC, Wanke CA, Greenblatt DJ. 2008. Ritonavir greatly impairs CYP3A activity in HIV infection with chronic viral hepatitis. *J Acquir Immune Defic Syndr* 49:358–368. <https://doi.org/10.1097/QAI.0b013e31818c7efe>.
 50. Dittmer DP, Damania B. 2016. Kaposi sarcoma-associated herpesvirus: immunobiology, oncogenesis, and therapy. *J Clin Invest* 126:3165–3175. <https://doi.org/10.1172/JCI84418>.
 51. Boss IW, Nadeau PE, Abbott JR, Yang Y, Mergia A, Renne R. 2011. A Kaposi's sarcoma-associated herpesvirus-encoded ortholog of microRNA miR-155 induces human splenic B-cell expansion in NOD/LtSz-scid IL2Rg^{amnull} mice. *J Virol* 85:9877–9886. <https://doi.org/10.1128/JVI.05558-11>.
 52. Skalsky RL, Samols MA, Plaisance KB, Boss IW, Riva A, Lopez MC, Baker HV, Renne R. 2007. Kaposi's sarcoma-associated herpesvirus encodes an ortholog of miR-155. *J Virol* 81:12836–12845. <https://doi.org/10.1128/JVI.01804-07>.
 53. Gottwein E, Mukherjee N, Sachse C, Frenzel C, Majoros WH, Chi JT, Braich R, Manoharan M, Soutschek J, Ohler U, Cullen BR. 2007. A viral microRNA functions as an orthologue of cellular miR-155. *Nature* 450:1096–1099. <https://doi.org/10.1038/nature05992>.
 54. Greenfield EA. 2015. Generating monoclonal antibodies, p 201–221. *In* Greenfield EA (ed), *Antibodies: a laboratory manual*, 2nd ed. Cold Spring Harbor Laboratory Press, Cold Spring Harbor, NY.

55. Lee BH, Gauna AE, Pauley KM, Park Y-J, Cha S. 2012. Animal models in autoimmune diseases: lessons learned from mouse models for Sjögren's syndrome. *Clin Rev Allergy Immunol* 42:35–44. <https://doi.org/10.1007/s12016-011-8288-5>.
56. Richman LP, Vonderheide RH. 2014. Role of crosslinking for agonistic CD40 monoclonal antibodies as immune therapy of cancer. *Cancer Immunol Res* 2:19–26. <https://doi.org/10.1158/2326-6066.CIR-13-0152>.
57. White AL, Chan HTC, Roghanian A, French RR, Mockridge CI, Tutt AL, Dixon SV, Ajona D, Verbeek JS, Al-Shamkhani A, Cragg MS, Beers SA, Glennie MJ. 2011. Interaction with FcγRIIB is critical for the agonistic activity of anti-CD40 monoclonal antibody. *J Immunol* 187:1754–1763. <https://doi.org/10.4049/jimmunol.1101135>.
58. Barr TA, McCormick AL, Carling J, Heath AW. 2003. A potent adjuvant effect of CD40 antibody attached to antigen. *Immunology* 109:87–92. <https://doi.org/10.1046/j.1365-2567.2003.01634.x>.
59. Martin C, Waghele SD, Lokhandwala S, Ambrus A, Bray J, Vuong C, Vinodkumar V, Dominowski PJ, Rai S, Mwangi D, Foss DL, Mwangi W. 2017. Characterization of a broadly reactive anti-CD40 agonistic monoclonal antibody for potential use as an adjuvant. *PLoS One* 12:e0170504. <https://doi.org/10.1371/journal.pone.0170504>.
60. Carling J, Szabo MJ, Dickinson R, De Leenheer E, Heath AW. 2012. Conjugation of lymphoma idiotype to CD40 antibody enhances lymphoma vaccine immunogenicity and antitumor effects in mice. *Blood* 119:2056–2065. <https://doi.org/10.1182/blood-2011-05-355461>.
61. Satoh M, Reeves WH. 1994. Induction of lupus-associated autoantibodies in BALB/c mice by intraperitoneal injection of pristane. *J Exp Med* 180:2341–2346. <https://doi.org/10.1084/jem.180.6.2341>.
62. Johnson SC, Yanos ME, Kayser EB, Quintana A, Sangesland M, Castanza A, Uhde L, Hui J, Wall VZ, Gagnidze A, Oh K, Wasko BM, Ramos FJ, Palmiter RD, Rabinovitch PS, Morgan PG, Sedensky MM, Kaeberlein M. 2013. mTOR inhibition alleviates mitochondrial disease in a mouse model of Leigh syndrome. *Science* 342:1524–1528. <https://doi.org/10.1126/science.1244360>.
63. Bride KL, Vincent T, Smith-Whitley K, Lambert MP, Blessing JJ, Seif AE, Manno CS, Casper J, Grupp SA, Teachey DT. 2016. Sirolimus is effective in relapsed/refractory autoimmune cytopenias: results of a prospective multi-institutional trial. *Blood* 127:17–28. <https://doi.org/10.1182/blood-2015-07-657981>.
64. Mukherjee S, Mukherjee U. 2009. A comprehensive review of immunosuppression used for liver transplantation. *J Transplant* 2009:701464. <https://doi.org/10.1155/2009/701464>.
65. Roy D, Sin SH, Lucas A, Venkataramanan R, Wang L, Eason A, Chavakula V, Hilton IB, Tamburro KM, Damania B, Dittmer DP. 2013. mTOR inhibitors block Kaposi sarcoma growth by inhibiting essential autocrine growth factors and tumor angiogenesis. *Cancer Res* 73:2235–2246. <https://doi.org/10.1158/0008-5472.CAN-12-1851>.
66. Brenchley JM, Price DA, Schacker TW, Asher TE, Silvestri G, Rao S, Kazzaz Z, Bornstein E, Lambotte O, Altmann D, Blazar BR, Rodriguez B, Teixeira Johnson L, Landay A, Martin JN, Hecht FM, Picker LJ, Lederman MM, Deeks SG, Douek DC. 2006. Microbial translocation is a cause of systemic immune activation in chronic HIV infection. *Nat Med* 12:1365–1371. <https://doi.org/10.1038/nm1511>.
67. Polizzotto MN, Uldrick TS, Wyvill KM, Aleman K, Marshall V, Wang V, Whitby D, Pittaluga S, Jaffe ES, Millo C, Tosato G, Little RF, Steinberg SM, Sereti I, Yarchoan R. 2016. Clinical features and outcomes of patients with symptomatic Kaposi sarcoma herpesvirus (KSHV)-associated inflammation: prospective characterization of KSHV inflammatory cytokine syndrome (KICS). *Clin Infect Dis* 62:730–738. <https://doi.org/10.1093/cid/civ996>.
68. Carbone A, De Paoli P, Gloghini A, Vaccher E. 2015. KSHV-associated multicentric Castlemans disease: a tangle of different entities requiring multitarget treatment strategies. *Int J Cancer* 137:251–261. <https://doi.org/10.1002/ijc.28923>.
69. Paiardini M, Müller-Trutwin M. 2013. HIV-associated chronic immune activation. *Immunol Rev* 254:78–101. <https://doi.org/10.1111/immr.12079>.
70. de Sanjose S, Mbisa G, Perez-Alvarez S, Benavente Y, Sukvirach S, Hieu NT, Shin HR, Anh PT, Thomas J, Lazzano E, Matos E, Herrero R, Munoz N, Molano M, Franceschi S, Whitby D. 2009. Geographic variation in the prevalence of Kaposi sarcoma-associated herpesvirus and risk factors for transmission. *J Infect Dis* 199:1449–1456. <https://doi.org/10.1086/598523>.
71. Matar CG, Anthony NR, O'Flaherty BM, Jacobs NT, Priyamvada L, Engwerda CR, Speck SH, Lamb TJ. 2015. Gammaherpesvirus co-infection with malaria suppresses anti-parasitic humoral immunity. *PLoS Pathog* 11:e1004858. <https://doi.org/10.1371/journal.ppat.1004858>.
72. MacDuff DA, Reese TA, Kimmey JM, Weiss LA, Song C, Zhang X, Kambal A, Duan E, Carrero JA, Boisson B, Laplantine E, Israel A, Picard C, Colonna M, Edelson BT, Sibley LD, Stallings CL, Casanova JL, Iwai K, Virgin HW. 2015. Phenotypic complementation of genetic immunodeficiency by chronic herpesvirus infection. *eLife* <https://doi.org/10.7554/eLife.04494>.
73. Barton ES, White DW, Cathelyn JS, Brett-McClellan KA, Engle M, Diamond MS, Miller VL, Virgin HW. 2007. Herpesvirus latency confers symbiotic protection from bacterial infection. *Nature* 447:326–329. <https://doi.org/10.1038/nature05762>.
74. Sin SH, Fakhari FD, Dittmer DP. 2010. The viral latency-associated nuclear antigen augments the B-cell response to antigen in vivo. *J Virol* 84:10653–10660. <https://doi.org/10.1128/JVI.00848-10>.
75. Müller JA, Harms M, Schubert A, Mayer B, Jansen S, Herbeuval J-P, Michel D, Mertens T, Vapalahti O, Schmidt-Chanasit J, Münch J. 2017. Development of a high-throughput colorimetric Zika virus infection assay. *Med Microbiol Immunol* 206:175–185. <https://doi.org/10.1007/s00430-017-0493-2>.
76. O'Hara AJ, Vahrsen W, Dittmer DP. 2008. Gene alteration and precursor and mature microRNA transcription changes contribute to the miRNA signature of primary effusion lymphoma. *Blood* 111:2347–2353. <https://doi.org/10.1182/blood-2007-08-104463>.